Quasioptical design of integrated Doppler backscattering and correlation electron cyclotron emission systems on the DIII-D tokamak

Citation: Rhodes, T. L. et al. "Quasioptical design of integrated Doppler backscattering and correlation electron cyclotron emission systems on the DIII-D tokamak." Review of Scientific Instruments 81(2010): 10D912. © 2010 American Institute of Physics

As Published: http://dx.doi.org/10.1063/1.3475797

Publisher: American Institute of Physics

Persistent URL: http://hdl.handle.net/1721.1/66099

Version: Final published version: final published article, as it appeared in a journal, conference proceedings, or other formally published context

Quasioptical design of integrated Doppler backscattering and correlation electron cyclotron emission systems on the DIII-D tokamak[a)]

T. L. Rhodes,[1,b)] W. A. Peebles,[1] X. Nguyen,[1] J. C. Hillesheim,[1] L. Schmitz,[1]
A. E. White,[2,c)] and G. Wang[1]
[1]*Department of Physics and Astronomy, University of California, Los Angeles, California 90098, USA*
[2]*Oak Ridge Institute for Science Education, Oak Ridge, Tennessee 37831-0117, USA*

(Presented 18 May 2010; received 12 May 2010; accepted 19 June 2010;
published online 8 October 2010)

The quasioptical design of a new integrated Doppler backscattering (DBS) and correlation electron cyclotron emission (CECE) system is presented. The design provides for simultaneous measurements of intermediate wavenumber density and long wavelength electron temperature turbulence behavior. The Doppler backscattering technique is sensitive to plasma turbulence flow and has been utilized to determine radial electric field, geodesic acoustic modes, zonal flows, and intermediate scale ($k \sim 1-6$ cm^{-1}) density turbulence. The correlation ECE system measures a second turbulent field, electron temperature fluctuations, and is sensitive to long poloidal wavelength ($k \leq 1.8$ cm^{-1}). The integrated system utilizes a newly installed in-vessel focusing mirror that produces a beam waist diameter of 3.5–5 cm in the plasma depending on the frequency. A single antenna (i.e., monostatic operation) is used for both launch and receive. The DBS wavenumber is selected via an adjustable launch angle and variable probing frequency. Due to the unique system design both positive and negative wavenumbers can be obtained, with a range of low to intermediate wavenumbers possible (approximately -3 to 10 cm^{-1}). A unique feature of the design is the ability to place the DBS and CECE measurements at the same radial and poloidal locations allowing for cross correlation studies (e.g., measurement of nT cross-phase).
 [doi:10.1063/1.3475797]

I. INTRODUCTION

The quasioptical design of a new integrated Doppler backscattering (DBS) and correlation electron cyclotron emission (CECE) system operating in the millimeter wave band (50–110 GHz) is presented in this paper. This integrated system addresses the diagnostic need to measure low through intermediate wavenumber density fluctuations as well as low wavenumber temperature fluctuations simultaneously. Multifield and multiscale fluctuation measurements such as these are believed vital in validation studies of gyrokinetic turbulence simulations and address significant questions regarding the roles that multiscale turbulence and zonal flows play in governing anomalous transport. Millimeter wave diagnostics are also believed to be applicable over a wide range of both existing and future fusion plasmas.

The system described here utilizes a newly installed focusing mirror located inside the vacuum vessel that produces a beam waist diameter of 3.5–5 cm in the plasma depending upon the probe frequency. A single antenna (i.e., monostatic operation) is used for both launch and receive. The DBS wavenumber is selected via an adjustable mirror launch angle and variable probing frequency. Due to the unique system design both positive and negative wavenumbers can be obtained, with low as well as intermediate wavenumbers possible (approximately -3 to 10 cm^{-1}). Another unique feature of the design is the ability to place the DBS and CECE measurements at the same radial and poloidal locations allowing for cross correlation studies (e.g., measurement of nT cross-phase). The system is installed on the DIII-D tokamak and has been providing a significant amount of data over the past year. For reference the DIII-D tokamak is a medium sized tokamak, with typical parameters of major radius $R=1.7$ m, minor radius $a=0.6$ m, magnetic field $B=0.6-2.1$ T, plasma current 1–2 MA, elongation $\kappa \sim 1-2$, $\sim$17.5 MW neutral beam injection, $\sim$3.5 MW electron cyclotron heating, and $\leq$3.6 MW fast wave heating.

The Doppler backscattering technique is sensitive to plasma turbulence flow and has been utilized to determine radial electric field, geodesic acoustic modes, zonal flows, and intermediate scale ($k \sim 1-6$ cm^{-1}) density turbulence levels.[1–4] The Doppler backscattering method consists of injecting a probe beam of a given frequency and polarization into a plasma which contains a cutoff for that frequency and polarization. The radiation is injected at an angle with respect to the cutoff layer and scatters from density fluctuations with the density fluctuation wavenumber satisfying the familiar Bragg scattering relation $\mathbf{k}_{\tilde{n}}=2\mathbf{k}_{\mathrm{local}}$. Here $\mathbf{k}_{\mathrm{local}}$ is the local wavevector (near the cutoff location) of the incident radiation which depends upon the launch angle, frequency,

[a)]Contributed paper, published as part of the Proceedings of the 18th Topical Conference on High-Temperature Plasma Diagnostics, Wildwood, New Jersey, May 2010.
[b)]Electronic mail: trhodes@ucla.edu.
[c)]Present address: Department of Nuclear Science and Engineering, Massachusetts Institute of Technology, Cambridge, Massachusetts.

and plasma index of refraction.[1–4] The Bragg relation is a vector relation and so scattering only occurs if the $\mathbf{k}_{\tilde{n}}$ is both present and is aligned along $\mathbf{k}_{\text{local}}$. An important feature of the backscattering process is that the backscattered power is related to the local fluctuation level at that particular $\mathbf{k}_{\tilde{n}}$. A fluctuation flow velocity in the direction of $\mathbf{k}_{\tilde{n}}$ creates a Doppler shift in the signal scattered from the density fluctuations. The local flow velocity $\mathbf{V}$ of the fluctuations can then be derived from knowledge of $\mathbf{k}_{\tilde{n}}$ and the measured frequency shift f_{Doppler} via $f_{\text{Doppler}}=2\mathbf{k}_{\text{local}}\cdot\mathbf{V}/2\pi$. Knowledge of the local wavenumber $\mathbf{k}_{\text{local}}$ is obtained from ray tracing calculations. The scattered signal is received by an antenna either diplexed with the launch antenna or located near the launch antenna. The Doppler frequency then typically depends upon both the background $E\times B$ velocity as well as the intrinsic propagation velocity of the fluctuations. It is often found (although not always) that the $E\times B$ velocity dominates in which case the measurement is a good estimate of local radial electric field. In that case fluctuations in the electric field can also appear as fluctuations in the Doppler shift frequency. The current DBS system operates in the frequency range of 50–75 GHz (V-band), utilizes quadrature detection, and can be configured in either O- or X-mode polarization.

Measurements of broadband core electron temperature fluctuations have been made on DIII-D using a CECE technique which is sensitive to long poloidal wavelength ($k\leq 1.8\ \text{cm}^{-1}$).[5–8] This technique is required since the observation of electron temperature fluctuations related to plasma turbulence requires differentiation from the thermal fluctuations inherent in the ECE signal. Currently, a two-channel correlation method is employed to discriminate the true temperature fluctuation from thermal ECE emission fluctuations. Tunable bandpass filters are used for the two channels. Electron temperature fluctuations related to plasma turbulence remain correlated if the bandpass filter spacing probes spatial locations separated less than the radial correlation length of the temperature fluctuations. In contrast, natural fluctuations of the ECE signal related to thermal emission are decorrelated provided the two filters do not overlap in frequency. Currently, the CECE system on DIII-D operates in the range ~80–105 GHz and uses the second harmonic ECE layer (X-mode).

II. SYSTEM DESIGN

The general layout of the quasioptical components of the system is shown in Fig. 1. The overall design goal was to form a high quality Gaussian beam in the core of DIII-D plasmas for a range of frequencies applicable to both V and W-band operation. The rotatable parabolic mirror serves to probe a range of wavenumber values with the DBS system. The two waveguide bands, V (50–75 GHz) and W (75–110 GHz), are combined using a Pacific Millimeter Products diplexer (m/n VWMUX) into a single V-band rectangular output. Diplexer single pass insertion losses are low, ~2 dB across both bands. A single Millitech V-band scalar antenna (m/n SFH-15-STP-25) is used to launch the V-band probe signal and also serves to receive both the V-band DBS signal and the W-band CECE signal. Single antenna operation (commonly referred to as monostatic operation) has several advantages over dual antenna (bistatic operation) including straightforward quasioptical design and analysis of the backscattered DBS signal as well as similar propagation paths for the DBS and CECE signals. Small dc offsets in the DBS quadrature signals due to internal reflections are handled by dc offsets in the amplifier section. The interested reader is referred to Ref. 9 for greater detail on the electronics (probe frequencies, quadrature mixers, etc.) of the DBS system and Ref. 8 for similar information on the CECE system. After the scalar antenna the beam propagates to a 26.7 cm diameter, f=48 cm aspheric high-density polyethylene (HDPE) lens which forms a parallel beam. A flat turning mirror directs the beam onto the parabolic mirror (f=130 cm) that then forms a beam waist inside the plasma, as shown in Fig. 1. Note that with the exception of the parabolic mirror all components are mounted on an optical table that is located outside the vessel. The external location of the antenna and lens provides significant flexibility to modify and optimize the system based on a given experimental requirement. For example, either X-mode or O-mode polarization can be chosen for the DBS system which provides a much higher range of accessible densities (note that the CECE system must be X-mode to access the second harmonic X-mode emission layer). The angle of the parabolic mirror and the resulting launch/receive angle are remotely controllable and can be varied from −10° to +2° on a shot to shot basis. A higher mirror angular range of −12° to +4° is possible; however the beam begins to interfere with the top and bottom port walls. The dotted lines in Fig. 1 are included as an illustration of a second angle. The angular variation allows the DBS system to probe a significant range of wavenumbers, ~0–6 cm^{-1} (Fig. 2). Larger wavenumbers can be accessed due to specific plasma shapes, e.g., a high triangularity plasma will present a larger range of possible angles as compared to a low triangularity plasma. For example, if the plasma shown in Fig. 1 were shifted downward the angle of the filled blue beam would increase with respect to the plasma boundary even though the launch angle remains the same. Due to the shaping flexibility of DIII-D the mirror angles must be selected based upon the desired wavenumbers and the particular plasma shape.

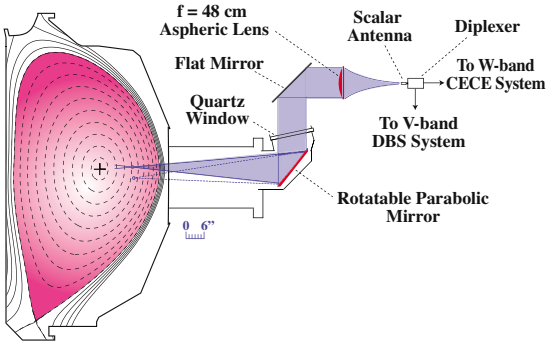

FIG. 1. (Color online) Geometry and layout of system. Outline of the DIII-D vacuum vessel shown with a representative plasma cross-section. Two beam launch angles are shown for reference, one in solid blue and the second with dotted blue lines.

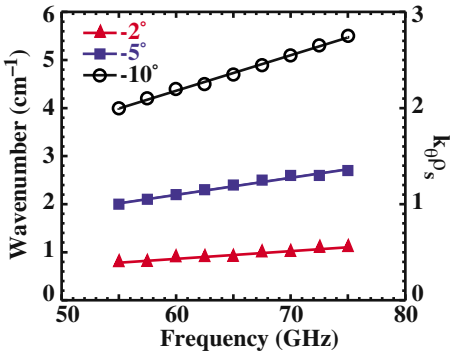

FIG. 2. (Color online) Typical DBS wavenumber access for a range of frequencies and launch angles. For reference the values of $k_\theta \rho_s$ are shown on the right hand axis (ρ_s is the ion Larmor radius using the local electron temperature with $\rho_s = 0.5$ cm used in this example). Note that only negative mirror angles are shown. Positive angles extend to +2° and give a symmetric wavenumber response for this example.

III. LABORATORY TESTS

The initial system design was performed using standard Gaussian ray propagation calculations and checked with optical ray tracing. A full-scale mockup was constructed for laboratory testing. The mockup system underwent a range of tests and optimizations to verify and characterize the design performance prior to final construction and installation on DIII-D. Comparison of the final Gaussian beam design to laboratory measurements is shown in Fig. 3. Note that the flat turning mirror is not shown in these calculations since it produces no change in the beam parameters. The W-band tests at 94 GHz show reasonable agreement between measured beam radii in the region of interest (z=270–320 cm) and laboratory measurements. A minimum beam waist of diameter $2w_0 \approx 3.5$ cm is found. Representative V-band tests at 58.6 GHz are shown in Fig. 3(b) where reasonable agreement is also seen with the exception of the point at $z \sim 261$ cm which appears too small compared to the predicted value. A beam diameter of $2w_0 \approx 5$ cm is seen in the region z=280–310. The radial location of either the DBS or CECE signal within the plasma depends upon the magnetic field **B** and density profiles (the ECE resonance depends on **B**, the X-mode cutoff depends on both **B** and density for

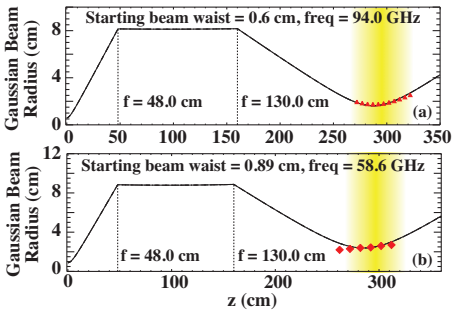

FIG. 3. (Color) Predictions from Gaussian beam calculations (black line) compared to laboratory measurements (red diamonds) for (a) W-band, 94 GHz, and (b) V-band, 58.6 GHz. The HDPE lens is represented by the line marked with focal length f=48 cm and the parabolic mirror by the line marked with focal length f=130 cm. Note that the x axes are slightly different. The yellow band indicates a typical plasma location ranging from the edge or separatrix to the plasma center

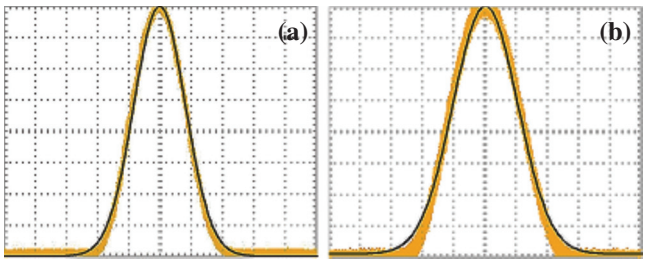

FIG. 4. (Color) Representative antenna beam patterns for (a) W-band profile, 94 GHz (b) V-band profile, 69.6 GHz. The scales are 1 cm per division. Data are yellow and Gaussian fit is black.

DBS, and the O-mode cutoff for DBS depends only on the density). The signal can then come from any location along the Gaussian profiles shown in Fig. 3. Thus it was important to match the beam waist to a typical range of plasma cutoff and resonance locations. In addition, the beam properties must remain reasonably constant over an appreciable radial range. From Fig. 3 it is seen that the beam widths have a small variation over a significant radial range, varying by ~15% over a ±18 cm range for the W-band and ±20 cm for V-band (this is a significant portion of the typical 60 cm DIII-D minor radius). For reference the Rayleigh range (the length over which the radius increases by ~40%) is larger at roughly ±30 and ±37.5 cm for W and V-band, respectively.

Representative beam profiles for W and V-band operation are shown in Fig. 4. These are taken at the beam waist location (z ~ 290 cm in Fig. 3) which is located near the plasma midradius when in operation. Gaussian fits are shown in black and the experimental data in yellow. The profiles are seen to be closely Gaussian in shape except near the beam edge where small deviations are observed. Note that these are beam profiles of the power, i.e., electric field squared. The Gaussian widths $2w_0$ are found to be 3.4 and 3.9 cm, respectively, for the 94 and 69.6 GHz profiles. The beam size and quality affect both the CECE and DBS system performance. The poloidal wavenumber range of the CECE system is determined by the beam size in the poloidal direction. It can be shown that the 1/e width of a Gaussian in real space (dr) transforms to the 1/e width in wavenumber space (dk) as $dk = 2/dr$. Thus a 1/e spot radius of $w_0 = 1.75$ cm gives a 1/e poloidal wavenumber range of $\leq 2/1.75 = 1.1$ cm^{-1}. Similarly the beam quality affects the DBS system performance with a relatively narrow waist often being the optimum solution for a broad range of plasma conditions and radii.[10] High quality CECE and DBS require negligible small side lobes as confirmed by measurement.

IV. REPRESENTATIVE DATA

In this section representative data illustrating the system capabilities are shown. The first example is a wavenumber spectrum obtained from a DBS wavenumber scan (Fig. 5). These data are from early in an Ohmic discharge (800 ms) with each wavenumber point taken from a separate, identical plasma discharge. The probe frequency is kept constant while the launch angle is changed, thus avoiding uncertainties associated with cross-calibrating different probe frequencies. A relatively steep falloff with k is observed that is not

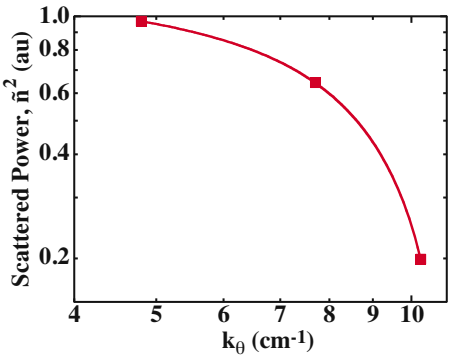

FIG. 5. (Color online) Wavenumber spectral scan from radial location $r/a \sim 0.35$. Note that the axes are log-log. The k range of 4.8–10.2 cm^{-1} corresponds to a $k\rho_s$ range of 1–2.1. The curve is a fit to guide the eye.

well described by a single power law k dependency in this wavenumber range. This wavenumber range is typical of the trapped electron mode instability. Data such as these significantly increase the number of constraints that gyrokinetic turbulence simulations must satisfy in validation studies and significantly add to such studies.

A second example shows the Doppler shift due to neutral beam injection (Fig. 6). Figure 6(a) shows the scattered signal ($\tilde{n}$) as a function of time and frequency. The radial location of the signal is approximately constant at $r/a \sim 0.8 (R_{major}=2.2$ m) for the time period 600–1200 ms. This is due to the approximately constant density during this time period. Between 1200 and 1400 ms there is a slow outward drift to $r/a \sim 0.86$ due to an increasing plasma density. Approximately 1.9 MW average neutral beam power is injected starting at 700 ms. Between 700 and 1200 ms the beams are modulated with a 35 ms on and 15 ms off pattern. A second modulated beam starting at 1200 ms increases the average power to 3.2 MW. The beam modulation can be seen as periodic shifts on the spectra and also on the mean Doppler shifted frequency $f_{Doppler}=\int fP(f)df$ [Fig. 6(b)]. For reference, the injected neutral beam power P_{inj} is also shown in Fig. 6(b). The DBS data show that the fluctuation flow velocity changes from the electron diamagnetic drift direction to the ion diamagnetic drift direction with the co-neutral

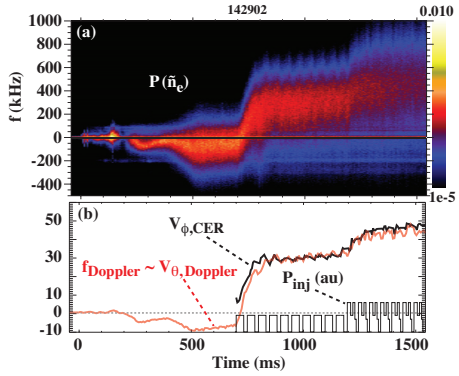

FIG. 6. (Color) (a) Scattered signal vs time and frequency showing response to changes in rotation associated with neutral beam injection. (b) Mean Doppler shifted frequency (proportional to $V_{\theta,Doppler}$ as explained in the text, in arbitrary units scaled to match $V_{\phi,CER}$ at 1000 ms) and toroidal rotation from a CER channel viewing a carbon impurity near the same radius. Also shown is injected neutral beam power in arbitrary units.

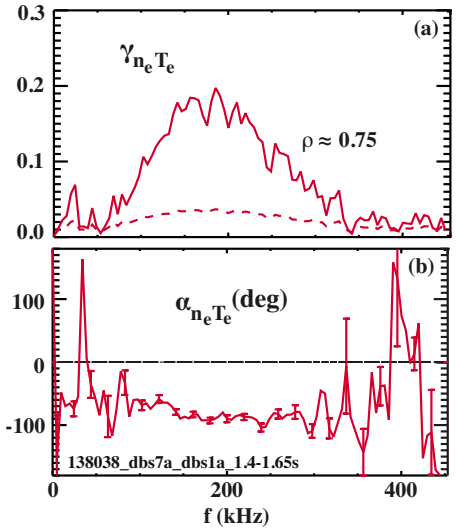

FIG. 7. (Color online) An example of the measured coherency γ_{neTe} and cross-phase angle α_{neTe} for radial location $\rho=0.75$ are shown in (a) and (b), respectively. Dashed line on the coherency plot indicates a statistical noise limit, error bars on the cross-phase angle are the one-sigma standard deviations, and a horizontal line at $\alpha_{neTe}=0°$ is for reference.

beam injection (NBI) at 700 ms. For comparison, the toroidal rotation from a charge exchange recombination (CER) channel viewing a carbon impurity at a radial location near that of the DBS signal is plotted along with the mean Doppler frequency $f_{Doppler}$ (proportional to $V_{\theta,Doppler}$) in Fig. 6(b). The core radial electric field is often dominated by the toroidal rotation so that comparing these two quantities is reasonable. Both show similar modulations due to the NBI modulation as well as a similar overall time history. The differences after ~1200 ms are attributed to an outward drift of the radial location of the DBS signal due to increasing plasma density.

A final example showing the cross correlation of density (from near horizontally launched DBS) and temperature fluctuations (from CECE) and the resulting cross-phase is shown in Fig. 7. As described earlier, the two signals share the same microwave path via the quasioptical system and have been overlapped in space by careful adjustment of the CECE frequency. The cross-phase comparisons of this measurement with theory and simulation provide valuable new information about the physics of turbulence.[12]

In conclusion, the system has been fully operational for approximately one year producing data for a variety of physics studies and has been especially useful for validation studies of gyrokinetic turbulence simulations (e.g., see Refs. 11 and 12). Other studies include toroidal correlations with a second DBS system separated 180° toroidally for identification of the n=0 properties of geodesic acoustic modes (GAMS) and zonal flows.[13] Finally, near term upgrades being considered to the quasioptical system include optimization of beam profile for scrape off layer (SOL) studies and quasioptical polarization combining for simultaneous O-mode DBS and X-mode CECE or for the addition of a second DBS system.

ACKNOWLEDGMENTS

Work is supported by the U.S. DOE under Grant Nos. DE-FG02-08ER54984 and DE-AC05-06OR23100.

[1] M. Hirsch, E. Holzhauer, J. Baldzuhn, B. Kurzan, and B. Scott, Plasma Phys. Controlled Fusion **43**, 1641 (2001).
[2] G. D. Conway and the ASDEX, Plasma Phys. Controlled Fusion **50**, 124026 (2008).
[3] P. Hennequin, C. Honoré, A. Truc, A. Quéméneur, N. Lemoine, J.-M. Chareau, and R. Sabot, Rev. Sci. Instrum. **75**, 3881 (2004).
[4] L. Schmitz, G. Wang, J. C. Hillesheim, T. L. Rhodes, W. A. Peebles, A. E. White, L. Zeng, T. A. Carter, and W. Solomon, Rev. Sci. Instrum. **79**, 10F113 (2008).
[5] G. Cima, R. V. Bravenec, A. J. Wootton, T. D. Rempel, R. F. Gandy, C. Watts, and M. Kwon, Phys. Plasmas **2**, 720 (1995).
[6] S. Sattler, H. J. Hartfuss, and W7-AS Team, Phys. Rev. Lett. **72**, 653 (1994).
[7] V. S. Udintsev, M. Goniche, J. L. Ségui, G. Giruzzi, D. Molina, F. Turco, G. T. A. Huysmans, P. Maget, Tore Supra Team, and A. Krämer-Flecken, Fusion Sci. Technol. **50**, 508 (2006).
[8] A. E. White, L. Schmitz, W. A. Peebles, T. A. Carter, T. L. Rhodes, E. J. Doyle, P. A. Gourdain, J. C. Hillesheim, G. Wang, C. Holland, G. R. Tynan, M. E. Austin, G. R. McKee, M. W. Shafer, K. H. Burrell, J. Candy, J. C. DeBoo, R. Prater, G. M. Staebler, R. E. Waltz, and M. A. Makowski, Rev. Sci. Instrum. **79**, 103505 (2008).
[9] J. C. Hillesheim, W. A. Peebles, T. L. Rhodes, L. Schmitz, T. A. Carter, P.-A. Gourdain, and G. Wang, Rev. Sci. Instrum. **80**, 083507 (2009).
[10] E. Blanco, T. Estrada, and J. Sánchez, Plasma Phys. Controlled Fusion **48**, 699 (2006).
[11] J. C. DeBoo, C. Holland, T. L. Rhodes, L. Schmitz, G. Wang, A. E. White, M. E. Austin, E. J. Doyle, J. Hillesheim, W. A. Peebles, C. C. Petty, Z. Yan, and L. Zeng, Phys. Plasmas **17**, 056105 (2010).
[12] A. E. White, W. A. Peebles, T. L. Rhodes, C. H. Holland, G. Wang, L. Schmitz, T. A. Carter, J. C. Hillesheim, E. J. Doyle, L. Zeng, G. R. McKee, G. M. Staebler, R. E. Waltz, J. C. DeBoo, C. C. Petty, and K. H. Burrell, Phys. Plasmas **17**, 056103 (2010).
[13] J. C. Hillesheim, W. A. Peebles, T. L. Rhodes, L. Schmitz, A. E. White, and T. A. Carter, Rev. Sci. Instrum. **81**, 10D907 (2010).